Article

Cell Reports

Quaternary Structure Defines a Large Class of Amyloid-β Oligomers Neutralized by Sequestration

Graphical Abstract

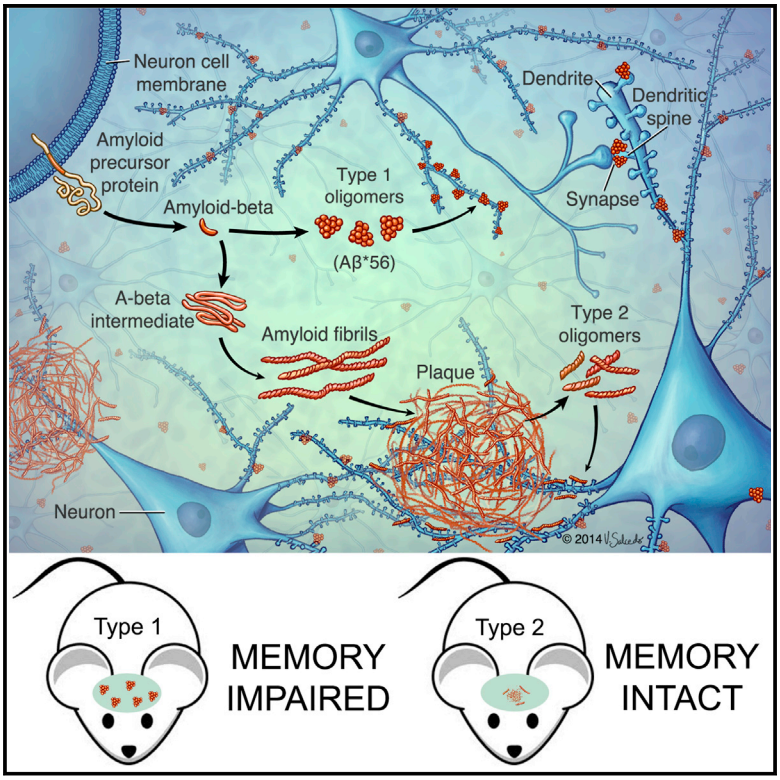

Highlights

- Brain-derived amyloid-β oligomers (Aβo) are classified as type 1 and type 2
- Type 1 Aβo, A11-immunoreactive, have no spatiotemporal relationship with Aβ plaques
- Type 2 Aβo, OC-immunoreactive, emerge after and accumulate around Aβ plaques
- Type 2 Aβo, despite being highly abundant, do not impair cognition in situ

Authors

Peng Liu, Miranda N. Reed, Linda A. Kotilinek, ..., James P. Cleary, Kathleen R. Zahs, Karen H. Ashe

Correspondence

hsiao005@umn.edu

In Brief

Liu et al. classify brain-derived amyloid-β oligomers into type 1 and type 2. Type 2, but not type 1, oligomers have a spatiotemporal and structural relationship with amyloid plaques. Highly abundant type 2 oligomers do not impair cognition in situ, possibly due to spatial sequestration around plaques.

Liu et al., 2015, Cell Reports *11*, 1760–1771
June 23, 2015 ©2015 The Authors
http://dx.doi.org/10.1016/j.celrep.2015.05.021

OPEN ACCESS
CellPress

Cell Reports
Article

Quaternary Structure Defines a Large Class of Amyloid-β Oligomers Neutralized by Sequestration

Peng Liu,[1,2] Miranda N. Reed,[1,2,9] Linda A. Kotilinek,[1,2] Marianne K.O. Grant,[1,2] Colleen L. Forster,[2,3] Wei Qiang,[7,10] Samantha L. Shapiro,[1,2] John H. Reichl,[1,2] Angie C.A. Chiang,[8] Joanna L. Jankowsky,[8] Carrie M. Wilmot,[5] James P. Cleary,[1,2,6] Kathleen R. Zahs,[1,2] and Karen H. Ashe[1,2,4,6,*]

[1]Department of Neurology
[2]N. Bud Grossman Center for Memory Research and Care
[3]UMN Academic Health Center Biological Materials Procurement Network
[4]Department of Neuroscience
[5]Department of Biochemistry, Molecular Biology and Biophysics
University of Minnesota, Minneapolis, MN 55455, USA
[6]Geriatric Research, Education and Clinical Center (GRECC), VA Medical Center, Minneapolis, MN 55417, USA
[7]Laboratory of Chemical Physics, National Institute of Diabetes and Digestive and Kidney Diseases, NIH, Bethesda, MD 20892, USA
[8]Departments of Neuroscience, Neurology and Neurosurgery, Huffington Center on Aging, Baylor College of Medicine, Houston, TX 77030, USA
[9]Present address: Department of Psychology, Behavioral Neuroscience, West Virginia University, Morgantown, WV 26506, USA
[10]Present address: Department of Chemistry, Binghamton University, Vestal, NY 13902, USA
*Correspondence: hsiao005@umn.edu
http://dx.doi.org/10.1016/j.celrep.2015.05.021

SUMMARY

The accumulation of amyloid-β (Aβ) as amyloid fibrils and toxic oligomers is an important step in the development of Alzheimer's disease (AD). However, there are numerous potentially toxic oligomers and little is known about their neurological effects when generated in the living brain. Here we show that Aβ oligomers can be assigned to one of at least two classes (type 1 and type 2) based on their temporal, spatial, and structural relationships to amyloid fibrils. The type 2 oligomers are related to amyloid fibrils and represent the majority of oligomers generated in vivo, but they remain confined to the vicinity of amyloid plaques and do not impair cognition at levels relevant to AD. Type 1 oligomers are unrelated to amyloid fibrils and may have greater potential to cause global neural dysfunction in AD because they are dispersed. These results refine our understanding of the pathogenicity of Aβ oligomers in vivo.

INTRODUCTION

Alzheimer's disease (AD) is believed to be caused by neurotoxic assemblies of the amyloid-β (Aβ) peptide. Distinct assemblies of Aβ have been found in the human brain, including amyloid fibrils and a few specific oligomers (Lasagna-Reeves et al., 2011; Lesné et al., 2013; Lu et al., 2013; Noguchi et al., 2009; Shankar et al., 2008). It is widely accepted that Aβ oligomers (Aβo) are more potent neurotoxins than amyloid fibrils, and several oligomers have been isolated and studied in detail. These oligomers differ in size and, to varying degrees, in their temporal and spatial patterns of expression, association with other brain proteins, and effects on neuronal function and viability (Lasagna-Reeves et al., 2011; Lesné et al., 2006, 2013; Noguchi et al., 2009; Shankar et al., 2008). However, there is no general consensus as to which oligomers are the most significant in the pathophysiology of AD nor, indeed, on the total number of Aβo types produced in the brain (reviewed in Benilova et al., 2012). The diversity of form and function among the Aβo studied thus far, and the likely existence of an indeterminate number of other Aβo, makes the isolation and functional characterization of all potential forms a laborious, if not impossible, task. In an attempt to resolve this predicament, we asked whether Aβo generated in vivo could be categorized according to their spatiotemporal patterns of expression and structural features as inferred from their reactivity with conformation-selective antibodies, and, if so, whether the different classes of oligomers exert different pathological effects on neural function.

Studies using conformation-selective antibodies have identified at least two classes of oligomers that are generated in vitro and in the brains of AD patients and amyloid precursor protein (APP) transgenic mice (Glabe, 2008). The OC and A11 conformation-selective antibodies detect mutually exclusive structural epitopes of amyloid-forming proteins, independent of primary amino acid sequence (Kayed et al., 2007; Wu et al., 2010). OC antibodies recognize Aβ amyloid fibrils as well as Aβo (Kayed et al., 2007); it has been suggested, but never directly demonstrated, that OC detects in-register parallel β sheets (Glabe, 2009; Wu et al., 2010). Conversely, A11 antibodies have been shown to recognize out-of-register anti-parallel β sheet structures (Laganowsky et al., 2012; Liu et al., 2012). Our objective in the current work was to address the following questions related to Aβo generated in vivo: (1) are there distinct subtypes of Aβo based on quaternary structural motifs, as

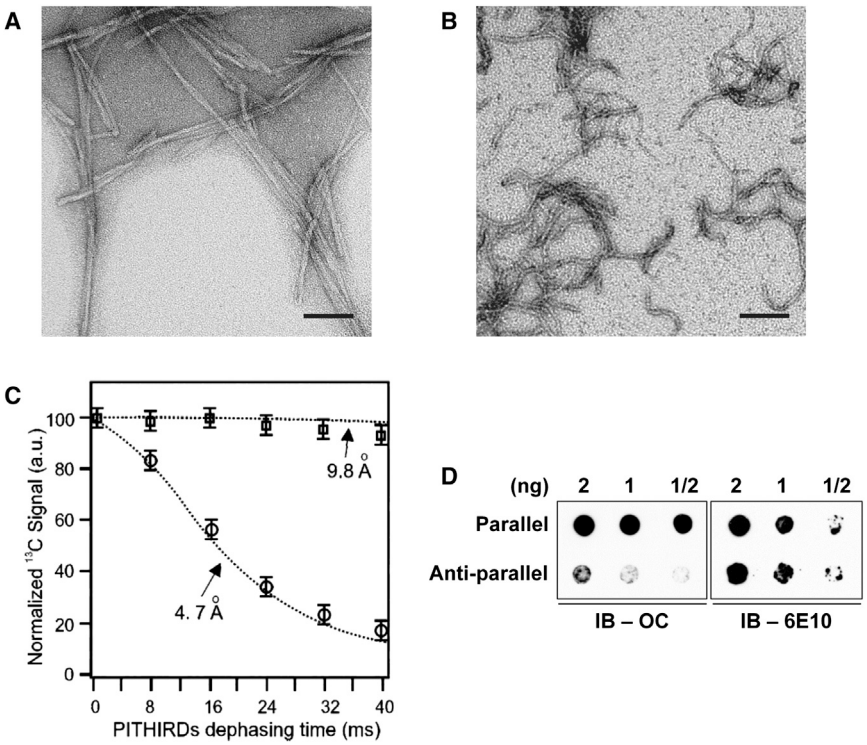

Figure 1. OC Antibodies Recognize In-Register Parallel β Sheet Structures

(A and B) Transmission electron micrographs show D23N_Aβ40 fibrils with (A) in-register parallel β sheet structure and (B) anti-parallel structure.

(C) ^{13}C-PITHIRDs-CT decay curves for parallel and anti-parallel fibrils with ^{13}C labeling at Ala21-^{13}C′. Theoretical decay curves with 4.7 and 9.8 Å ^{13}C-^{13}C distances are shown as dotted lines. Experimental data for the parallel and anti-parallel fibrils are indicated by circles and squares, respectively. The error bars (SEM) were determined from the experimental spectral noise.

(D) (Left) Dot blot shows that OC antibodies selectively detect D23N_Aβ40 fibrils with in-register parallel β sheet structure. (Right) Blot shown at left was stripped and re-probed with monoclonal antibody 6E10 to confirm that approximately equal amounts of parallel and anti-parallel fibrils were loaded. Scale bars (A and B), 100 nm. See also Figure S1.

defined by their reactivity with OC and A11 antibodies; (2) do OC- and A11-reactive oligomers differ in their spatial and temporal patterns of appearance; and (3) what is the most abundant type of Aβo produced in the brain and how does it affect neurological function?

To address these questions, we employed transgenic mice expressing APP variants linked to AD. The types of Aβo (e.g., Aβ dimers and Aβ*56, a putative dodecamer) and fibrils in mice vary dynamically, over a timescale of weeks to months (for examples in Tg2576, Arc6, and hAPP-J20 mice, see Cheng et al., 2007; Lesné et al., 2006; and Shankar et al., 2009). In the lines that have been characterized, the sequence of appearance of specific Aβ assemblies is consistent. Here we studied four lines of transgenic mice. In Tg2576 (Hsiao et al., 1996), hAPP-J20 (Cheng et al., 2007), and TetO-APP$_{SweInd}$ mice (Jankowsky et al., 2005), the A11-reactive oligomer Aβ*56 appeared in young mice ~3–6 months prior to dense-core plaques and correlated with spatial memory deficits (Cheng et al., 2007; Fowler et al., 2014; Lesné et al., 2006). In rTg9191 mice (Liu et al., 2015), we found dense-core plaques emerging at ~12 months, but no Aβ*56 at any age (Liu et al., 2015).

Here we show that OC antibodies selectively recognized quaternary structural motifs found in naturally occurring Aβ amyloid fibrils, namely in-register parallel β sheets (for review, see Glabe, 2009 and Tycko, 2011). We also show that OC-immunoreactive Aβo appeared only after plaque formation and that they were highly concentrated around amyloid plaques in the brains of APP transgenic mice. Conversely, A11-immunoreactive oligomers appeared prior to amyloid plaques in multiple lines of APP transgenic mice (here and see also Cheng et al., 2007; Fowler et al., 2014; and Lesné et al., 2006), and they were dispersed in the brain parenchyma without any relationship to amyloid plaques. We classified the Aβo generated in the brains of these APP transgenic mice into two categories: (1) type 1, which has no temporal, spatial, or structural relationship to amyloid fibrils; and (2) type 2, which is related to amyloid fibrils temporally, spatially, and structurally. We found that in brains bearing dense-core plaques, type 2 Aβo predominate, consistent with predictions from in vitro studies (Cohen et al., 2013). However, type 2 Aβo appear to have limited potential to diffuse away from dense-core plaques or to disrupt forebrain neural networks, as assessed by tests of cognition.

RESULTS

OC Antibodies Selectively Detect In-Register Parallel β Sheet Structures

We first sought to more precisely define the structures recognized by OC and A11 antibodies. It was not possible to isolate from the brains of transgenic mice Aβo of sufficient purity or quantity to perform biophysical characterization of their structures, so we turned to synthetically prepared Aβ fibrils with defined quaternary structures. It had been suggested that OC detects in-register parallel β sheets (Glabe, 2009; Wu et al., 2010), but this hypothesis had not been directly tested. Amyloid fibrils containing in-register parallel β sheets or anti-parallel β sheets were prepared from the 40-residue Aβ peptide with the AD-linked Iowa mutation (D23N_Aβ40). Transmission electron microscopy and solid-state nuclear magnetic resonance spectroscopy confirmed that these fibrils had the morphological features of parallel and anti-parallel fibrils whose backbone registries in the hydrophobic core regions were defined (Qiang et al., 2012; Sgourakis et al., 2015; Figures 1A–1C). OC antibodies

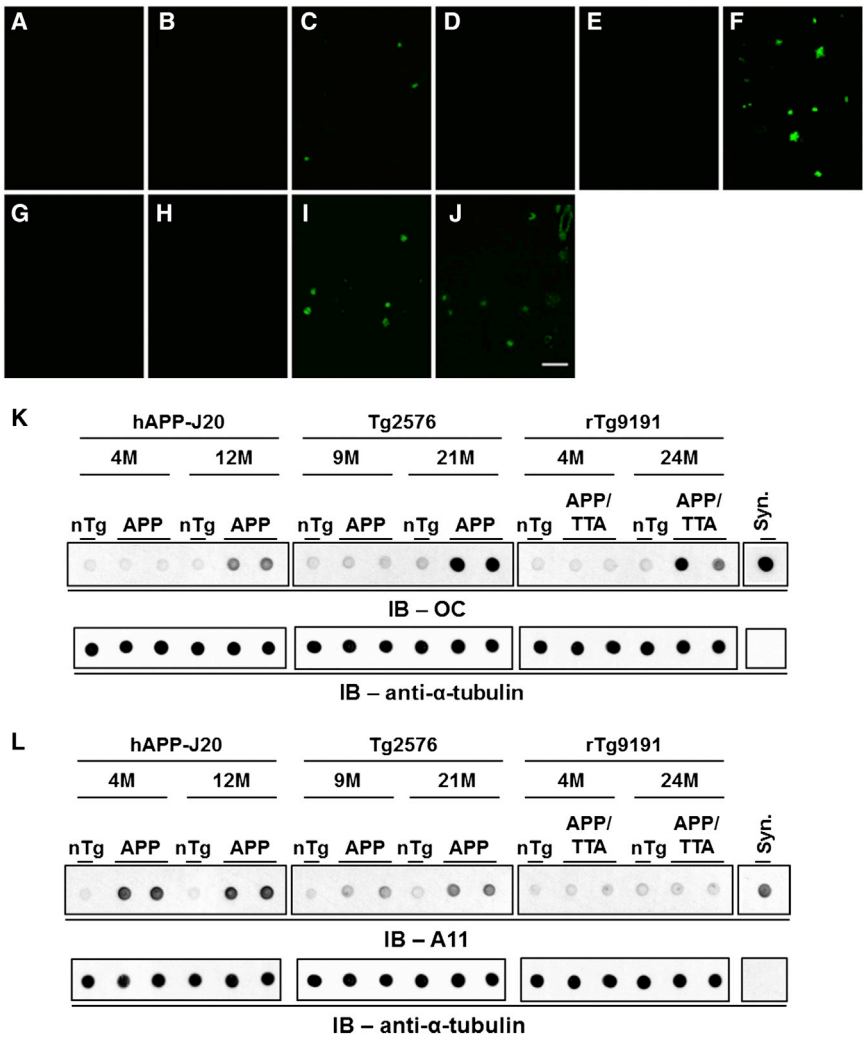

Figure 2. Age-Dependent Appearance of A11- and OC-Immunoreactive Aβo

(A–J) Brain sections stained with thioflavin S reveal dense-core plaques in cerebral cortex. (A–C) hAPP-J20 (A, non-transgenic, 4 months; B, hAPP-J20, 4 months; C, hAPP-J20, 12 months); (D–F) Tg2576 (D, non-transgenic, 9 months; E, Tg2576, 9 months; F, Tg2576, 21 months); (G–I) rTg9191 (G, non-transgenic, 4 months; H, rTg9191, 4 months; I, rTg9191, 24 months); (J) AD brain. Scale bar in (J), 100 μm, applies to (A–J).

(K) OC-reactive aggregates are seen after the appearance of dense-core plaques. (Top) Dot blots show protein aggregates detected by polyclonal OC antibodies in water-soluble brain extracts from hAPP-J20, Tg2576, and rTg9191 mice prior to (hAPP-J20, 4 months; Tg2576, 9 months; rTg9191, 4 months) and after (hAPP-J20, 12 months; Tg2576, 21 months; rTg9191, 24 months) the appearance of dense-core plaques. Extracts from non-transgenic littermates (nTg) are shown for comparison. Synthetic soluble Aβ aggregates (syn) with in-register parallel β sheets (2 ng) were used as a positive control. (Bottom) α-tubulin served as the loading control.

(L) A11-reactive aggregates are seen prior to the appearance of dense-core plaques. (Top) Dot blots were prepared as in (K) but probed with A11 antibodies. Synthetic Aβ40 oligomers (syn) were prepared as in Kayed et al. (2003). (Bottom) α-tubulin served as the loading control. See also Figures S2 and S7.

preferentially recognized parallel, over anti-parallel, fibrils in immunoblots (Figure 1D).

It also has been suggested that A11 antibodies recognize structures containing anti-parallel β sheets (Glabe, 2009; Wu et al., 2010), and A11 indeed reacts with synthetic oligomers composed of out-of-register anti-parallel β sheets (Laganowsky et al., 2012; Liu et al., 2012). We first tested whether A11 antibodies prefer anti-parallel over parallel β sheets, using synthetic Aβ fibrils. A11 antibodies also detected these synthetic fibrils, although with less sensitivity than did OC (Figure S1A). Similar to OC, A11 preferred parallel fibrils to anti-parallel fibrils. While this result might seem at odds with the notion of two structurally distinct classes of oligomers, a potential resolution may be found in Figure S1B. We compared the A11 signal generated by synthetic Aβ fibrils to the signal generated by Aβo in the brains of 4-month-old hAPP-J20 mice, which lack OC-reactive Aβ species (see below). A much stronger signal was observed from the brain extracts, estimated to contain ~3 pg *total* Aβ, based on semi-quantitative analysis of Aβ in western blots (data not shown) and previously reported ELISA measurements of Aβ levels in hAPP-J20 mice at this age (Cheng et al., 2007), than from nanogram quantities of the synthetic Aβ fibrils. We concluded that while A11 can bind amyloid fibrils, it preferentially recognizes some structural feature of the brain-derived Aβo that is not found in fibrils containing in-register β sheets.

A11 Antibodies Recognize Aβo prior to Plaque Formation, while OC Antibodies Recognize Aβo Only after Plaques Appear

Aqueous extracts were prepared from the brains of Tg2576, hAPP-J20, and rTg9191 APP transgenic mice at ages prior to and following the appearance of dense-core plaques (Figures 2A–2J), and they were subjected to immunoblotting under non-denaturing conditions. OC immunoreactivity was seen only in extracts from plaque-containing brains in all three lines examined (Figures 2K and 6A; see also Liu et al., 2015). Conversely, A11 immunoreactivity appeared prior to plaque deposition in Tg2576 and hAPP-J20 mice and remained present in plaque-bearing brains (Figure 2L); no A11 immunoreactivity was observed in rTg9191 brain extracts from any age (Figures 2L, S2A, and S2B; Liu et al., 2015). A11 and OC immunoreactivity disappeared when extracts were immunodepleted of Aβ using a mixture of Aβ antibodies prior to immunoblotting (Figures

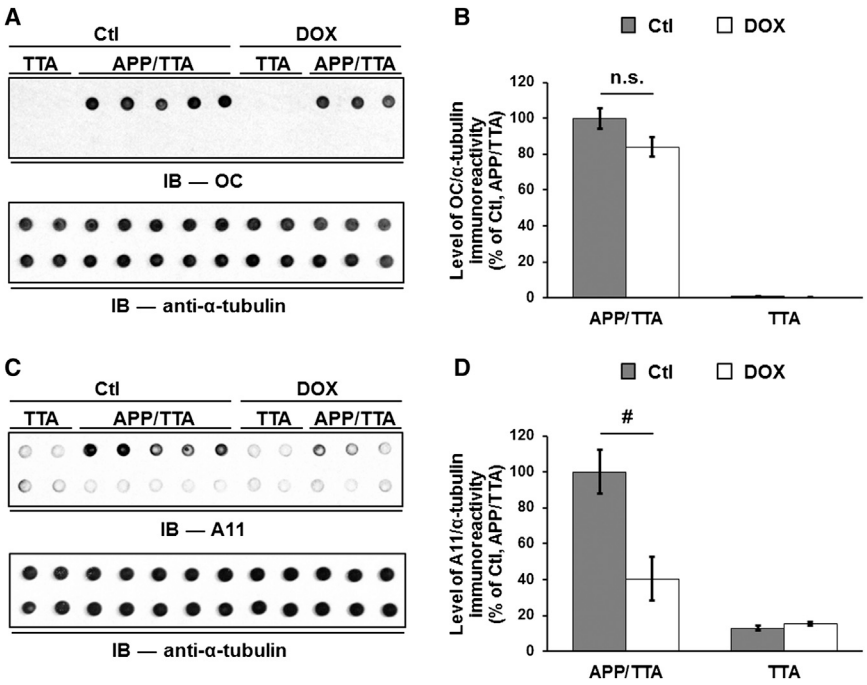

Figure 3. Suppression of Transgenic APP Selectively Lowers A11-Immunoreactive Aβo in TetO-APP$_{SweInd}$ Mice

(A) (Top) Protein aggregates detected by OC antibodies in aqueous brain extracts prepared from 8.5-month-old TetO-APP$_{SweInd}$ mice harboring both activator and responder transgenes (APP/TTA) or only the activator transgene (TTA). DOX, mice administered doxycycline to suppress APP expression for the 5 weeks immediately preceding sacrifice; Ctl, untreated mice; upper lane, brain extracts; lower lane, brain extracts immunodepleted of Aβ. (Bottom) α-tubulin served as the loading control.

(B) Quantification of OC immunoreactivity. There is no difference between levels of OC immunoreactivity, normalized to α-tubulin levels, in extracts from control (Ctl) and DOX-treated mice.

(C) (Top) Protein aggregates detected by A11 in the extracts described in (A) are shown. Upper lane, brain extracts; lower lane, brain extracts immunodepleted of Aβ. (Bottom) α-tubulin served as the loading control.

(D) Quantification of A11 immunoreactivity. Suppression of transgenic APP expression in TetO-APP$_{SweInd}$ mice resulted in an ~60% reduction in the levels of A11-reactive oligomers. n.s., not significant; #$p < 0.05$, two-way ANOVA followed by Fisher's post hoc analysis; error bars represent SEM. See also Figure S7.

S2C and S2D), demonstrating that the oligomers seen by A11 and OC in the brains of APP transgenic mice were indeed composed of Aβ. These results show that A11 and OC antibodies recognize different structures generated in vivo, as there exist brain-derived Aβ assemblies that are A11-positive/OC-negative (in young Tg2576 and hAPP-J20 mice) or OC-positive/A11-negative (in rTg9191 mice), extending the findings that OC and A11 recognize mutually exclusive epitopes on synthetic Aβo generated in vitro (Kayed et al., 2007; Wu et al., 2010).

Reducing APP in Plaque-Bearing Mice Selectively Lowers A11-Reactive Aβo

Tg2576, hAPP-J20, TetO-APP$_{SweInd}$, and rTg9191 mice express human APP at levels that vary among lines and contain one or more variants (Swedish in Tg2576, both Swedish and Indiana in hAPP-J20 and TetO-APP$_{SweInd}$, and both Swedish and London in rTg9191). These alterations result in different levels and amino acid compositions of Aβ, which we hypothesize contribute to the variability in the amount and types of Aβo generated, by analogy with in vitro studies. To determine whether the amount of Aβ expressed does indeed affect the relative levels of A11- and OC-reactive Aβo, we turned to TetO-APP$_{SweInd}$ mice. These mice carry a regulatable APP transgene, allowing us to manipulate levels of APP expression and, hence, levels of Aβ. When APP expression was suppressed by 90% for 5 weeks in plaque-bearing TetO-APP$_{SweInd}$ mice, TBS-soluble A11-reactive species decreased 60%, but TBS-soluble OC-reactive species remained stable (Figure 3). These results support the hypothesis that, in the presence of amyloid fibrils, the reaction kinetics favor the generation of OC-reactive over A11-reactive Aβo.

Type 2 Aβo Are Concentrated around Dense-Core Plaques and Occupy Only a Small Fraction of the Cortex

We went on to use OC antibodies to detect Aβo in the brains of two mouse models: rTg9191 and Tg2576. We found that brains of both rTg9191 and Tg2576 mice showed areas of intense OC immunoreactivity encircling Congo red-positive dense plaque cores (Figure S3A). In contrast to dense-core plaques, we found no OC reactivity in diffuse plaques lacking dense cores and plaque-associated cytopathology (Serrano-Pozo et al., 2011).

Since immunohistological methods are not optimally suited to measure finely dispersed molecules, it is possible that we did not detect low concentrations of OC-immunoreactive Aβo located outside the immediate vicinity of dense-core plaques. We therefore performed biochemical analyses on microdissected brain tissue fractions to more accurately define the spatial distribution of OC-immunoreactive Aβo and to discriminate between insoluble and soluble OC-immunoreactive assemblies.

Using laser microdissection, we isolated three tissue fractions in rTg9191 mice: (1) dense plaque cores containing Aβ fibrils; (2) halos extending 50 μm from the edge of the plaque cores; and (3) plaque-free zones, annuli extending 80–100 μm from the outer edges of the halos (Figure 4A). We opted to use autofluorescence rather than thioflavin S to identify candidate dense-core plaques, because thioflavin S artificially generated SDS-stable oligomers (Figure S3B). We performed control studies to verify the identity of autofluorescent structures by thioflavin S and Aβ immunohistochemistry using 4G8 (Figure S3C). We then measured native Aβ assemblies in each tissue fraction in dot blots using OC antibodies, and we found >99.9% of immunoreactivity confined to the cores and halos (Figures 4B and 4C).

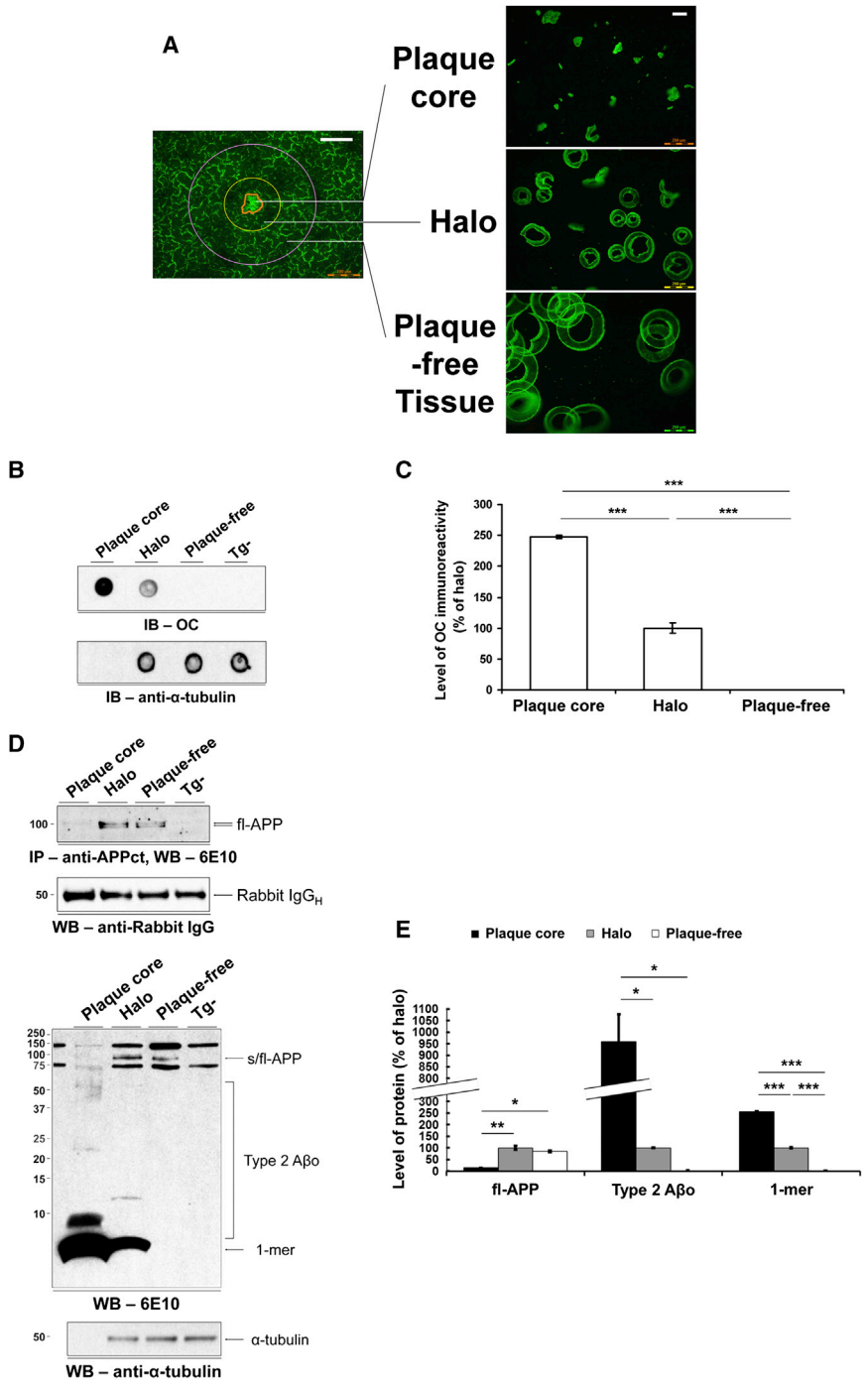

Figure 4. Type 2 Aβo Are Confined to Dense-Core Plaques in rTg9191 Mice

(A) Photomicrographs show microdissected fractions. White scale bars, 100 μm.

(B) (Top) Dot blot, probed with OC antibodies, illustrates the topographical distribution of native type 2 Aβo. (Bottom) Above blot was stripped and re-probed with anti-α-tubulin, showing that equal amounts of protein were loaded for the halo and plaque-free regions.

(C) Quantification of dot blots. OC-reactive aggregates are confined to the dense-core and halo regions.

(D) Immunoblotting under denaturing conditions confirms that type 2 Aβo are restricted to the dense-core and halo regions. (Top) Western blot shows full-length APP (fl-APP) in detergent-soluble extracts of laser-microdissected fractions. Fl-APP was immunoprecipitated with a polyclonal antibody directed against a C-terminal epitope in APP (anti-APPct) and detected using 6E10; blot was stripped and re-probed with an antibody directed against rabbit immunoglobulin (IgG), showing that approximately equal amounts of capture antibody were immunoprecipitated. (Bottom) Western blot was probed with monoclonal antibody 6E10; blot was stripped and re-probed with anti-α-tubulin.

(E) Quantification of western blots. Type 2 Aβo and monomers reside in the dense-core and halo regions, while fl-APP is primarily found in halo and plaque-free regions. *$p < 0.01$, **$p < 0.001$, ***$p < 0.0001$, one-way ANOVA followed by Fisher's post hoc analysis; error bars represent SEM. 1-mer, Aβ monomer; s/fl-APP, soluble and full-length amyloid precursor protein; Tg-, non-transgenic littermates of rTg9191 mice; IgG$_H$, immunoglobulin heavy chain. See also Figures S3, S4, and S7.

OC-immunoreactive Aβo thus are spatially, as well as temporally, associated with amyloid fibrils in the brains of APP transgenic mice. Further, OC-immunoreactive Aβo very probably share the in-register parallel β sheet structure that is characteristic of brain-derived amyloid fibrils (Lu et al., 2013). The spatial and temporal patterns of appearance of OC-immunoreactive oligomers strongly support the hypothesis that these oligomers form via a process of secondary self-assembly dependent upon pre-existing amyloid fibrils (see Discussion and Figure S7). We hereafter refer to OC-positive oligomers that exhibit spatial and temporal relationships to amyloid fibrils as type 2 Aβo. The laser microdissection results indicated that approximately all OC-immunoreactive Aβo in the brains of rTg9191 mice meet the spatial criterion for type 2 oligomers.

We next asked what fraction of the cortex is occupied by type 2 oligomers. Based on stereological analyses of thioflavin S-stained sections and the geometry of dense-core plaques (see the Supplemental Experimental Procedures), we estimated the volume of the cortex occupied by type 2 Aβo in rTg9191 mice to be 11.4%; therefore, >99.9% of the OC-immunoreactive Aβo in rTg9191 mice was confined to 11.4% of the cortex.

To measure other potential soluble Aβ assemblies in rTg9191 brains, we solubilized the Aβ assemblies from each tissue fraction in detergents, fractionated them by SDS-PAGE (which denatures the assemblies, as described below), and detected

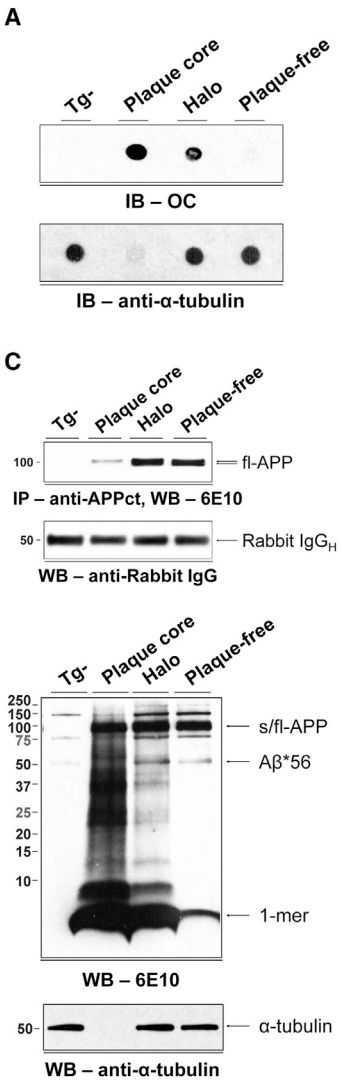

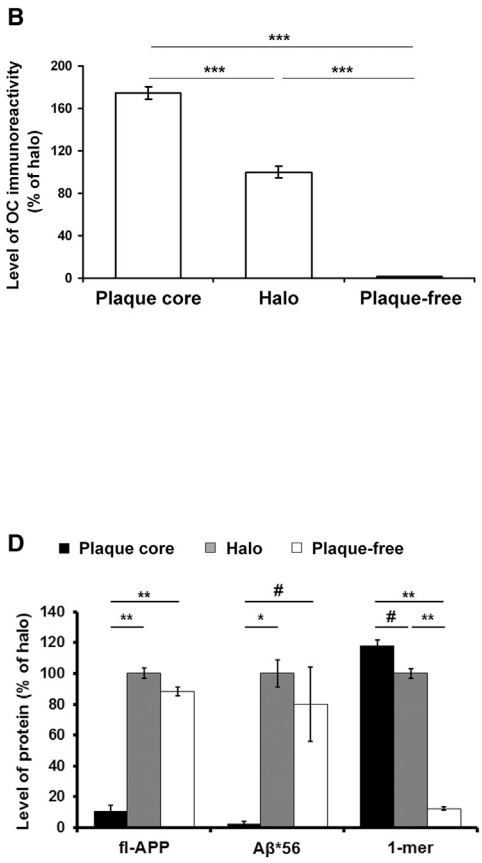

Figure 5. Type 2 Aβo and Aβ*56 Have Different Spatial Distributions in the Brains of Tg2576 Mice

(A) (Top) Dot blot probed with OC antibodies shows the topographical distribution of type 2 Aβo. (Bottom) α-tubulin blot shows that equal amounts of protein were loaded for the halo and plaque-free regions.

(B) Quantification of dot blots. Type 2 Aβo overwhelmingly reside in the dense-core and halo regions.

(C) (Top) Western blot shows fl-APP in detergent-soluble extracts of laser-microdissected fractions; blot was stripped and re-probed with anti-rabbit IgG antibody, showing that approximately equal amounts of capture antibody were immunoprecipitated. (Bottom) Western blot probed with 6E10 antibody shows the topographical distributions of APP, Aβ*56, and monomers (1-mer); α-tubulin blot shows that equivalent amounts of protein were loaded in the halo and plaque-free lanes.

(D) Quantification of western blots. Aβ*56 and fl-APP are primarily found in halo and plaque-free regions. In contrast, Aβ monomers overwhelmingly reside in the dense-core and halo regions. #$p < 0.05$, *$p < 0.01$, **$p < 0.001$, ***$p < 0.0001$, one-way ANOVA followed by Fisher's post hoc analysis; error bars represent SEM. Tg-, non-transgenic littermates of Tg2576; other abbreviations as in Figure 4. See also Figures S3, S4, and S7.

the denatured Aβ assemblies by immunoblotting with two different anti-Aβ antibodies (6E10, Figure 4D; 4G8, Figure S4A). We found an array of Aβ species in the cores and halos, but no Aβ assemblies in the plaque-free fraction. In addition, we found a strong concordance between measurements of the percentage of soluble Aβ assemblies located in the cores and halos obtained from dot blots with OC antibodies (>99.9%, Figure 4C) and measurements obtained from western blots with the two anti-Aβ antibodies (≥99.6%, Figures 4E and S4B), suggesting that all, or nearly all, of the soluble Aβo in rTg9191 mice is type 2 Aβo.

In additional biochemical studies, we found that when extracts of rTg9191 brains containing native type 2 Aβo were fractionated by size-exclusion chromatography and subsequently denatured by SDS-PAGE, Aβ species appeared in immunoblots as monomers, dimers, and larger oligomers (Figure S4C). Dimers were the most abundant Aβ oligomeric species in the immunoblots and eluted in two distinct sets of fractions; one set of fractions corresponded to the molecular masses of globular proteins ranging from ~500 to ~2,000 kDa, while the other set of fractions corresponded to ~60 to ~200 kDa proteins. We inferred from these results that the dimers in the immunoblots of denatured rTg9191 brain extracts represent disassembled high-molecular-mass type 2 Aβo, but we cannot exclude the existence of free non-globular dimers with larger radii of hydration than would be expected for a globular protein with a molecular mass of ~9 kDa, the theoretical molecular mass of dimers.

The Type 1 Aβ Oligomer Aβ*56 Is Distributed throughout the Cortex

The A11-immunoreactive oligomer Aβ*56 appears months before the emergence of the first detectable dense-core plaques in Tg2576 (Kawarabayashi et al., 2001; Lesné et al., 2006) and hAPP-J20 (Cheng et al., 2007; Wright et al., 2013) mice. We used Tg2576 mice, in which Aβ*56 was originally described (Lesné et al., 2006), to compare the spatial distribution of Aβ*56 to that of type 2 Aβo. We analyzed microdissected tissue fractions by dot blotting and western blotting (Figures 5A, 5C, and S4D). In quantitative analyses, we found a striking divergence in the distribution of OC-immunoreactive Aβo and Aβ*56: 99.5% of OC-immunoreactive Aβo was concentrated within plaque cores and halos (Figure 5B), whereas most of the Aβ*56 (≥98.7%) was distributed outside the core, in the halo and plaque-free zone (Figures 5D and S4E). We estimated that

Table 1. The Relative Levels and Spatial Occupancy of Type 1 and Type 2 Aβo in Aged Tg2576 Mice

Type of Aβo	Protein Level (ng/g brain tissue)	Percentage of Cortex Occupied
Type 2	14,500 ± 1,500[a]	13.9[b]
Aβ*56 (type 1)	57 ± 2[c]	98.4[b]
Total Aβ	15,200 ± 7,000[d]	NA

See also Figures S5 and S7. NA, not applicable.
[a]See Figure S5A.
[b]See Supplemental Experimental Procedures for calculations.
[c]See Figure S5B, assuming stoichiometry of 6E10:Aβ*56 is 12:1.
[d]See Figure S5C for calculations.

type 2 Aβo and Aβ*56 occupy 13.9% and 98.4%, respectively, of the volume of the cortex we sampled in aged Tg2576 mice (see the Supplemental Experimental Procedures).

Thus, in contrast to type 2 Aβo, Aβ*56 differs from amyloid fibrils in its temporal expression; spatial distribution; and quaternary structure, as inferred from its immunoreactivity with conformation-selective antibodies. We hereafter refer to A11-positive oligomers that appear independently of amyloid fibrils as type 1 Aβo.

Type 2 Aβo Levels Greatly Exceed Those of the Type 1 Oligomer Aβ*56 in Aqueous Brain Extracts from Tg2576 Mice

To determine the relative abundance of type 2 Aβo and Aβ*56, we estimated their masses in aqueous brain extracts from 21-month-old Tg2576 mice. To ascertain the Aβ content of type 2 Aβo, we compared OC immunoreactivity of extracts to that of synthetically produced in-register parallel β sheet Aβ fibrils containing known quantities of Aβ (measured by ELISA using 6E10 antibodies, following denaturation with hexa-fluoro-isopropanol [HFIP]). This method assumes that the relationship between OC immunoreactivity and Aβ content is the same for the synthetic fibrils and brain-derived type 2 Aβo. Using this method, type 2 oligomers were found to contain 14,500 ± 1,500 ng Aβ per gram of brain tissue. Levels of Aβ*56 were assessed by comparing the density of the 56-kDa band to known quantities of synthetic Aβ monomers on western blots probed with 6E10. This method assumes that the affinity of the 6E10 antibody was the same for the Aβ peptides within Aβ*56 as for the synthetic Aβ in blots subjected to antigen retrieval prior to incubation with 6E10. Our estimate of the amount of Aβ*56 depended on the stoichiometry of antibody binding to the synthetic standards and to Aβ*56. We assumed a stoichiometry of antibody:Aβ monomer of 1:1. Each molecule of Aβ*56, a putative Aβ dodecamer, could bind between 1 and 12 antibody molecules. Under the assumption that one molecule of Aβ*56 binds 12 antibodies (i.e., a 1:1 antibody:monomeric sub-unit ratio), we found that Aβ*56 contains 57 ± 2 ng Aβ per gram of brain tissue. However, this value could be as much as 12 times higher, if only one antibody binds to each molecule of Aβ*56. Finally, the total mass of Aβ ($Aβ_{x-38}$, $Aβ_{x-40}$, and $Aβ_{x-42}$) in the extracts was measured by ELISA using 6E10 antibodies, following denaturation with formic acid. We found that the total Aβ in aqueous extracts from aged Tg2576 mice is comprised of 0.4%–4.8% Aβ*56 and ~95% type 2 Aβo (Table 1; Figure S5).

Mice Producing Only Type 2 Aβo Are Cognitively Intact

Multiple studies have shown a correlation between the type 1 Aβo Aβ*56 and memory dysfunction in transgenic mice (Billings et al., 2007; Cheng et al., 2007; Lesné et al., 2006). The rTg9191 mice provided the opportunity to test the effects of type 2 Aβo on cognition, as rTg9191 mice produce type 2 Aβo exclusively. We studied cognitive function in rTg9191 mice that were aged until 21–24 months, when the relative quantity of type 2 Aβo in the brain, as assessed in dot blots using OC antibodies, was comparable to that in AD patients (Figures 6A and 6B). In a cohort of mice tested at 23 months, we found no significant transgene-associated effects on cognitive performance in the fixed consecutive number (FCN) task, an operant behavioral task sensitive to lesions of the prefrontal cortex (van Haaren et al., 1988; Figure 6C). Similarly, we found no significant impairment of spatial memory in any of three other cohorts of mice (young [4 months], middle-aged [12 months], and old [21 months]), evaluated using a water maze test of spatial reference memory that is sensitive to hippocampal lesions (Morris, 2007; Figure 6D). When the cohort of old mice was re-tested at 24 months, when levels of type 2 Aβo were significantly higher than in 21-month-old mice, there was still no decrement in performance (Table S1). Furthermore, there were no significant differences in performances between the old cohort (21 months old) and the other two cohorts (Figure 6D; Table S1). The slight increase in the proximity index (Table S1) and decrease in target-quadrant occupancy in the old mice appeared to be related to aging, since the same decrease can be seen in old, non-transgenic littermates (Figure 6D). Based on OC immunoreactivity in dot blots, the levels of type 2 Aβo in 24-month-old mice were 25- and 2.1-fold greater (calculated after subtracting background immunoreactivity observed in non-transgenic mice) than those in 4- and 12-month-old mice, respectively (Figure 6B). In summary, within the statistical limits of our measurements, there were no differences in cognitive function between mice with type 2 Aβo (at levels comparable to those in humans with AD), non-transgenic mice, and young rTg9191 mice with few or no such oligomers.

Type 2 Aβo Impair Cognition when Dispersed and Tested in Rats

The absence of any impact on cognitive function of type 2 Aβo produced in situ suggests that type 2 Aβo sequestered within dense-core plaques do not interfere with global network function, or that compensatory neural reorganization effectively preserves brain function when the oligomers occupy <15% of the cortex. It is possible that the background strain (129FVBF1) of rTg9191 is not permissive for the disruptive effects of Aβ on cognition, but this is unlikely because Tg2576 mice in the same background strain showed spatial memory deficits (Kotilinek et al., 2008). We also considered the possibility that the type 2 Aβo produced by rTg9191 mice lacked neurotoxicity. To test this hypothesis, we prepared aqueous protein extracts containing type 2 Aβo from the brains of 26-month-old rTg9191 mice, and we injected the extracts into the lateral cerebral ventricles of rats previously trained in a delayed non-matching-to-place

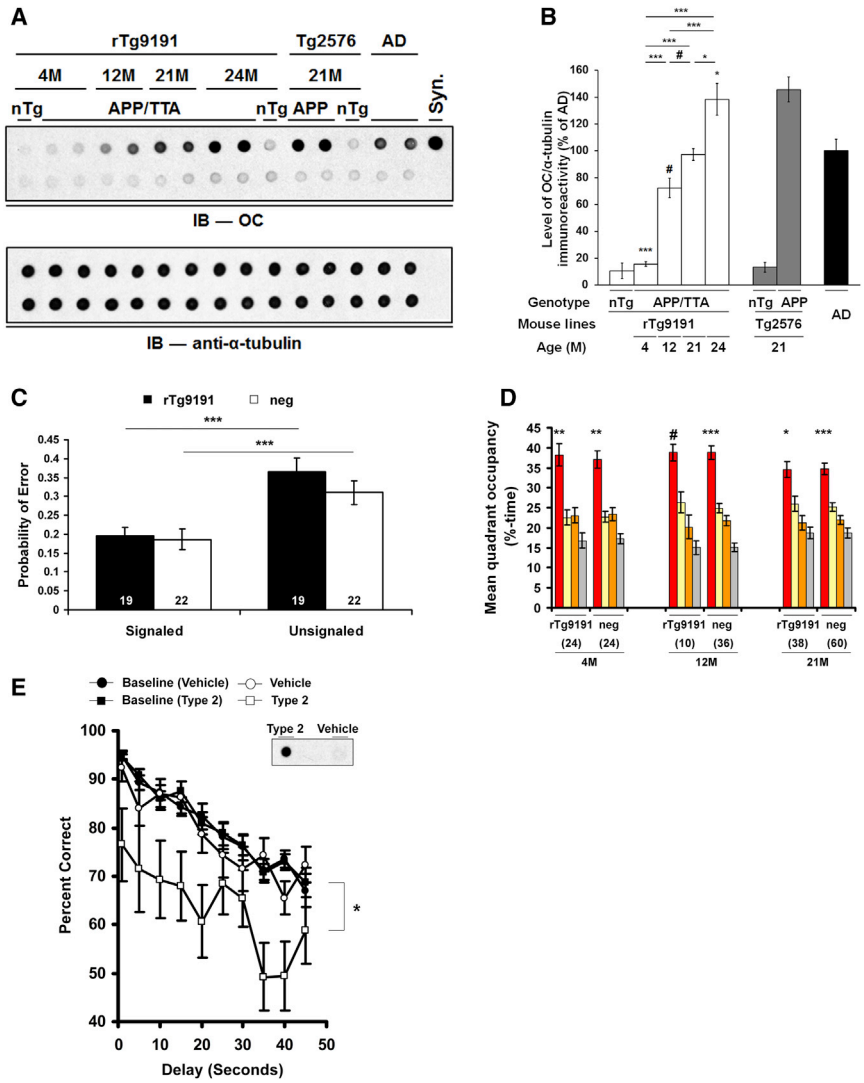

Figure 6. Type 2 Aβo Do Not Disrupt Cognition when Located In Situ in rTg9191 Brains, but Do Impair Cognition when Dispersed

(A–D) rTg9191 mice producing levels of type 2 Aβo comparable to those of AD patients have intact cognition. (A) (Top) Dot blot shows the relative levels of soluble OC-reactive aggregates in the brains of rTg9191 mice, non-transgenic littermates (nTg) and AD patients. Ages of mice are shown above the blot. Upper lane, water-soluble brain extracts and synthetic aggregates; lower lane, samples immunodepleted of Aβ; syn, synthetic soluble Aβ aggregates with in-register parallel β sheets. (Bottom) α-tubulin served as the loading control for both the untreated (upper lane) and Aβ-immunodepleted extracts (lower lane).

(B) Quantification of dot blots. Levels of OC-reactive aggregates in the brains of rTg9191 mice increase with age (#$p < 0.05$, *$p < 0.01$, ***$p < 0.0001$, one-way ANOVA followed by Fisher's post hoc analysis).

(C) Cognitive performance in 23-month-old APP-positive (rTg9191) and -negative (neg) rTg9191 mice do not differ in the signaled and unsignaled components of the FCN-4 test. The probability of a given trial producing an error in the signaled component is significantly lower than in the unsignaled component, indicating intact motor and visual function (***$p < 0.0001$, paired t test).

(D) Spatial reference memory in rTg9191 mice does not differ significantly from that of APP-neg littermates. Young (4 months), middle-aged (12 months), and old (21 months) mice were tested in the water maze; mean percentage time in each quadrant (target, red; left of target, yellow; right of target, orange; and opposite the target, gray) is shown. Significant search biases favoring the target quadrant were found in both rTg9191 mice and APP-neg littermates at all three ages. #$p < 0.05$, *$p < 0.01$, **$p < 0.001$, ***$p < 0.0001$, percentage time spent in the target compared to that in each of the other three quadrants, repeated-measures ANOVA (RM-ANOVA) followed by Fisher's post hoc analysis. Numerals in (C) and (D) represent the number of mice tested.

(E) Water-soluble brain extracts of rTg9191 mice containing type 2 Aβo disrupt cognition when exogenously administered to rats. Rats (n = 18) previously trained on a delayed non-matching–to-place task were injected intracerebroventricularly with brain extracts of rTg9191 mice containing type 2 Aβo or with extracts immunodepleted of Aβ (vehicle). Type 2 Aβo, but not vehicle, injections impaired performance on this task (*$p < 0.01$, RMANOVA compared to baseline performance [mean of three contiguous sessions]). (Inset) Dot blot shows OC immunoreactivity in type 2 Aβo-containing (type 2) and immunodepleted (vehicle) injectates. In (B–E), error bars represent SEM. See also Figure S6 and Table S1.

task, a test of short-term working memory (Paule et al., 1998). Each rat sequentially received brain extracts containing ~0% (Aβ immunodepletion), ~0.1% (low dose), or ~1% (high dose) of the total amount of type 2 Aβo in a 26-month-old rTg9191 mouse, and was tested 2 hr after the injections. Compared to baseline performance, memory was significantly impaired when rats were injected with the high dose of Aβ-containing extracts, but not when rats received the low dose or extracts from which Aβ was depleted (Figures 6E and S6). These results indicate that normal cognition in rTg9191 mice is probably not due to the lack of neurotoxicity of type 2 Aβo, since extracts containing minute quantities of dispersed type 2 Aβo disrupted cognition. These findings support the conclusion that spatial localization is a more significant determinant of the neurological effects of Aβo than overall abundance.

DISCUSSION

The data in this paper indicate that brain-derived Aβo can be categorized based on distinct temporal, spatial, and structural relationships to fibrils. Type 2 Aβo are observed only after dense-core plaque formation, are highly concentrated around dense-core plaques, and are recognized by OC antibodies, which we here show selectively bind to structures containing in-register parallel β sheets. The in-register parallel β sheet conformation is characteristic of all known naturally occurring Aβ fibrils (for review, see Glabe, 2009 and Tycko, 2011), so it

appears that type 2 Aβo and Aβ fibrils share a common quaternary structure. By contrast, type 1 Aβo are present both prior to and following the appearance of dense-core plaques, are dispersed in brain tissue, and are recognized by A11 antibodies. Importantly, these two classes of Aβo are differentially associated with impaired cognition: the type 1 Aβo Aβ*56 is associated with memory dysfunction in APP transgenic mice (Billings et al., 2007; Cheng et al., 2007; Lesné et al., 2006, 2008), while mice with levels of type 2 oligomers similar to those of AD patients have intact cognition. These results are summarized in Table S2. Taken together, these findings refine our understanding of how Aβo are organized and impact global neural network function in the brain.

The results of recently reported behavioral studies in TetO-APP_{SweInd} mice are consistent with our conclusion that type 2 Aβo are less harmful to neurological function than type 1 Aβo (Fowler et al., 2014). Using TetO-APP_{SweInd} mice of the identical age and strain background, exposed to the same dose of doxycycline for the same amount of time as the mice used here, Fowler et al. (2014) showed that 90% suppression of APP expression led to cognitive improvement, assayed with multiple behavioral tests. Cognitive improvement in these mice was accompanied by significant reductions in the level of A11-immunoreactive species generally, and in the level of Aβ*56 particularly, with no changes in amyloid plaque burden. In the current study, we have confirmed the findings of Fowler et al. (2014), showing that suppression of APP leads to reductions in A11-immunoreacitve species, and we have extended these findings to show that levels of OC-immunoreactive Aβo are unchanged. To summarize, an experimental manipulation that reduces levels of A11-reactive Aβo, while preserving levels of OC-reactive Aβo, leads to cognitive improvement in TetO-APP_{SweInd} mice.

We hypothesize that the differences in the spatiotemporal distributions of type 1 and type 2 Aβo result from distinct modes of biogenesis. Aβo have been shown in vitro to form via one of two processes: (1) primary self-assembly occurring independently of amyloid fibrils, or (2) secondary self-assembly requiring pre-existing fibrils that catalyze the self-assembly of monomers (Cohen et al., 2013; Figure S7). If these processes also occur in vivo, Aβo formed via secondary self-assembly should be seen only in brains containing amyloid fibrils and should be at highest concentration in the immediate vicinity of foci of Aβ fibrils (i.e., dense-core plaques). We propose that type 2 Aβo are generated by a secondary self-assembly process, because they appear only after dense-core plaques are present and they are highly concentrated around these plaques. Conversely, Aβo that form via primary self-assembly may be present prior to plaque formation and need not be concentrated around plaques—characteristics of type 1 Aβo, as defined here.

The two-pathway model of the self-assembly of Aβ (Figure S7) can explain the quantitative differences between type 1 and type 2 Aβo reported here. In vitro studies have shown that, in the presence of amyloid fibrils, reaction kinetics favor the generation of oligomers via a secondary self-assembly process (Cohen et al., 2013). After amyloid fibrils form in vitro, Aβ monomers are consumed by the elongation of fibrils and the secondary self-assembly reaction; if the consumption of monomers by these processes exceeds the production of Aβ monomers needed to form Aβo via primary self-assembly, then Aβo formed by primary self-assembly will decline or disappear. This model predicts that type 2 Aβo should predominate in plaque-bearing brains; indeed, type 2 Aβo are the most abundant Aβo in aged Tg2576 mice, comprising ~95% of the Aβ species in aqueous brain extracts from Tg2576 mice (with plaque loads slightly higher than those found in AD). The model also anticipates our result in vivo in TetO-APP_{SweInd} mice: when we reduced the pool of monomers by lowering APP expression, levels of type 1 Aβo fell but levels of type 2 Aβo remained unchanged. Finally, the presence of type 1 Aβo in Tg2576 mice and absence in rTg9191 mice also are consistent with this model. Tg2576 mice express more total Aβ than rTg9191 mice, but relatively less fibrillogenic Aβ42, because Tg2576 lack the *London* mutation; therefore, more monomers are available to form type 1 Aβo in Tg2576 than in rTg9191 mice.

Surprisingly, the prolific type 2 Aβo were not dispersed throughout brain tissue, but were instead encapsulated around dense-core plaques that in total occupied <15% of the cortex. Within this microenvironment, type 2 Aβo very likely cause neurodegenerative changes such as dystrophic neurites. It was shown previously that anti-Aβ immunotherapy reverses plaque-associated neuritic abnormalities without affecting plaque burden (Rozkalne et al., 2009), strongly suggesting that soluble Aβo cause cytopathology. Our rTg9191 mice, which generate only type 2 Aβo, exhibited plaque-associated cytopathology (Liu et al., 2015), yet remained cognitively normal. Thus, the encapsulation of type 2 Aβo in cyst-like dense-core plaques appears to neutralize their potential to disrupt neurological function. These results indicate that the spatial localization of Aβo is critically important, certainly more important than their overall abundance.

To evaluate the relevance of our findings to AD, we estimated the volume of human cortex occupied by type 2 Aβo in AD, using two different methods. One method depended on immunohistological data of tissue stained with the Aβo-specific antibody NAB-61 (Lee et al., 2006), which we inferred selectively recognizes type 2 Aβo and amyloid fibrils from its almost exclusive staining of neuritic plaques (dense-core plaques associated with neuritic abnormalities [Serrano-Pozo et al., 2011]). The average volume of AD cortex occupied by Aβ assemblies detected using NAB-61 was ~5% (Perez-Nievas et al., 2013). The other method relied on neuritic plaque densities. We estimated that the upper limit of the volume of cortex occupied by neuritic plaques in AD brain is ~10% (see the Supplemental Experimental Procedures). Both estimates were smaller than those in the Tg2576 and rTg9191 mouse model systems studied here, suggesting that, in humans, type 2 Aβo influence a relatively small volume of cortex and, as in the mice, would participate little if at all in disrupting cognition or inducing widespread neurodegeneration. However, we cannot exclude the possibility that type 2 Aβo might disrupt intrinsic connectivity networks in AD if higher-than-average concentrations of neuritic plaques accumulate in critical nodes. Nor can we conclude with certainty that type 1 Aβo levels are equivalent across all brain regions; for example, within a given region, local rates of Aβ production may be affected by neural activity (Cirrito et al., 2005; Kamenetz et al., 2003), which might alter the kinetics of self-assembly. A better understanding of the roles of type 1 and type 2 Aβo in

AD might be gained by comparing their respective levels in brain regions that are differentially vulnerable to neurodegenerative and functional abnormalities.

Although the biological factors involved in maintaining the sequestration of type 2 Aβo in dense-core plaques are not well understood, neuroinflammation seems to be important. While type 2 Aβo are smaller and, therefore, more diffusible than amyloid fibrils, their diffusion range may be circumscribed by microglial cells that may seal them inside amyloid plaques (Bolmont et al., 2008), thus potentially limiting their influence on brain function. It is possible that the compartmentalization eventually breaks down in symptomatic AD patients, allowing type 2 Aβo to leak out and damage a broader population of neurons. If type 2 Aβo in AD are as neurotoxic as those in rTg9191 mice, our results indicate that small breaches allowing only ~1% to pass through the putative barrier might be sufficient to disrupt global network function. Actual quantification is needed to test the hypothesis directly, but the poor correlation among neuritic plaques, β-amyloidosis, and cognition in humans (Katzman et al., 1988; Terry et al., 1991) argues against this possibility.

The uncertainty about which Aβo contribute to the pathogenesis of AD is a major impediment to progress on disease prevention, treatment, and diagnosis. Apparently conflicting results obtained in clinical trials of anti-amyloid therapies highlight the need for a more complete understanding of the types and toxicity of Aβ assemblies that are seen during the progression of AD. Passive immunization with two monoclonal antibodies that recognize Aβ fibrils, bapineuzumab and gantenerumab, reduced amyloid burdens but failed to provide cognitive or functional benefits (Alzforum, 2015a, 2015b; Ostrowitzki et al., 2012; Rinne et al., 2010). However, preliminary reports that a third antibody, aducanumab, practically eliminates plaques *and* slows cognitive and functional declines in patients with prodromal or mild AD have generated tremendous excitement in the field (Strobel, 2015). Aducanumab reportedly is highly selective for Aβo over Aβ monomers, but further details of the conformational selectivity of the antibody have not been made public. Taken together with the findings in mice reported here, the results of the clinical trials raise several questions. How did the stage at which therapy was administered, the degree of target engagement, and/or the precise identities of Aβ species targeted contribute to the differences in the outcomes of the clinical trials? Does aducanumab discriminate between type 1 and type 2 Aβo, as defined here, or does it recognize an epitope common to both types of Aβo? Does the microlocalization of different structural classes of Aβo in human brain parallel that seen in the brains of APP transgenic mice, reported here, and does this spatial distribution change during the progression of AD from the prodromal phase to dementia? Are there regions of the human brain where type 2 Aβo reach a high enough concentration to disrupt network function (the critical nodes mentioned above)?

In summary, the findings reported here suggest that, while most of the soluble Aβ in brains bearing dense-core plaques (e.g., AD brains) are type 2 Aβo, the bulk of these oligomers are rendered functionally innocuous by their effective containment within plaques. Type 1 Aβo may be more directly pathogenic in many brain regions because they are more finely dispersed than type 2 Aβo. We hope that our findings will open up new directions of research, particularly in understanding and developing therapies that target the rarer type 1 Aβo. A better understanding of how type 1 and type 2 Aβo impact the pathogenesis of AD may result from the synthesis of future biophysical and biological studies.

EXPERIMENTAL PROCEDURES

Animals

The rTg9191 mice were generated using a binary system of responder and activator transgenes (Paulson et al., 2008). Tg2576 mice (Hsiao et al., 1996) in a B6SJLF1 background (Westerman et al., 2002) and 4-month-old hAPPJ20 mice in a C57Bl6 background were from K.H.A.'s colony at the University of Minnesota. TetO-APP_{SweInd} mice in a B6FVB F1 background were from J.L.J.'s laboratory at Baylor College of Medicine. Brains from 12-month-old hAPP-J20 were a gift from Dr. Lennart Mucke of the University of California, San Francisco. All experiments involving mice and rats were conducted in full accordance with the Association for Assessment and Accreditation of Laboratory Animal Care and the Institutional Animal Care and Use Committee guidelines at the University of Minnesota, Minneapolis Veterans Administration Medical Center, or Baylor College of Medicine.

Human Brain Tissue

De-identified samples of inferior temporal gyrus (Brodmann Area 20) from individuals with a clinical diagnosis of AD were obtained from the Religious Orders Study (Rush Alzheimer's Disease Center). The Religious Orders Study is approved by the Institutional Review Board of Rush University Medical Center.

Sample Preparation for Parallel and Anti-parallel Fibrils and Synthetic Aβo

Details of preparation procedures are provided in the Supplemental Experimental Procedures.

Protein Extraction and Immunoblotting

To extract native Aβ aggregates, water-soluble extracts were prepared based on a protocol previously described (Shankar et al., 2008). Briefly, tissue specimens were weighed and transferred to 4 vol ice-cold buffer (25 mM Tris-HCl [pH 7.4], 140 mM NaCl, 3 mM KCl, 0.1 mM PMSF, 0.2 mM 1,10-phenanthroline monohydrate, protease inhibitor cocktail [Sigma-Aldrich], and phosphatase inhibitor cocktails [Sigma-Aldrich]) and homogenized using a Dounce homogenizer. The resulting materials were centrifuged for 90 min (16,100 × *g*, 4°C); the supernatant was depleted of endogenous immunoglobulins and stored at −20°C until further use.

Details of the dot blotting method are provided in the Supplemental Experimental Procedures. Briefly, 0.5 μg protein from brain extracts or 0.02–2 ng synthetic Aβ fibrils (Qiang et al., 2012) was spotted onto nitrocellulose membranes, which were then probed with either OC (Millipore, AB2286, 1:50,000) or A11 (Invitrogen, AHB0052, 1:1,000) antibodies.

Detergent-soluble Aβ species were extracted and western blotting was performed using the method of Liu et al. (2011).

Microdissection

Details of microdissection are provided in the Supplemental Experimental Procedures. Native and detergent-soluble proteins were extracted as described above; to compare protein levels in the microdissected fractions, extracts from equal volumes of tissue were used in dot blots and western blots. For negative controls, protein extracts from age-matched, nontransgenic littermates were loaded such that the total protein content equaled that of the plaque-free regions used for each blot.

Behavioral Tests

Details of the behavioral tests are provided in the Supplemental Experimental Procedures.

FCN Task

Forty-one (19 rTg9191, 22 neg) mice completed training under this assay. Mice were 20.5 months old at the start of training. After training, mice were run under the FCN-4 5 days/week for 30 daily sessions.

Water Maze

Spatial reference memory was measured in rTg9191 mice using a modified version of a water maze tailored to more rapid learning in the 129S6/FVB background strain and more sensitive to subtle deficits (Westerman et al., 2002). The rTg9191 mice (female and male) were tested cross-sectionally at 4 and 12 months of age, and longitudinally from 21 to 24 months. The spatial cues and hidden platform location were changed for the mice tested longitudinally at 24 months of age. Illness and spontaneous deaths were observed at the 21–24 month time point (4/60 neg and 6/40 rTg9191 mice; chi square, $p = 0.15$). Mice requiring euthanasia were not included in the analysis. The power of our study was sufficient to have an 80% chance of detecting an eight-point drop in mean percentage target quadrant occupancy at a confidence level of 0.05.

Delayed Non-Matching-to-Place Task

Twenty male Sprague-Dawley rats previously trained on a delayed non-matching-to-place task were injected intracerebroventricularly with brain extracts through chronically implanted guide cannulae (Reed et al., 2011). Each rat received 10 μl brain extract, prepared using the protocol for native aggregates described above; control extracts were prepared by two rounds of immunodepletion with monoclonal antibody 4G8. Animals were tested 2 hr post-injection. Each animal received injections of both fibril-dependent Aβo-containing and control extracts, on different days.

The task yields an accuracy-by-delay relationship, with high accuracy (percentage of correct responses) at the short delays and near random performance (50% correct) at the longest delays. This relationship is shifted leftward (working memory deficit) by compounds or conditions that adversely affect cognition. Performance on the day of injection was compared to baseline performance, defined as the mean of the scores at each delay (percentage of correct choices) for 3 days contiguous to the day of injection. Two animals that lost their cannulae were excluded from the analysis.

Histology and Immunohistochemistry

Details of histological procedures are provided in the Supplemental Experimental Procedures.

Statistics

Statistics were performed using StatView Version 5.0.1 (SAS Institute). Data are expressed as mean ± SEM.

SUPPLEMENTAL INFORMATION

Supplemental Information includes Supplemental Experimental Procedures, seven figures, and two tables and can be found with this article online at http://dx.doi.org/10.1016/j.celrep.2015.05.021.

AUTHOR CONTRIBUTIONS

P.L., K.R.Z., and K.H.A. conceived the project. P.L. planned and performed the biochemistry experiments, including characterization of the rTg9191 mice and laser microdissection, and analyzed the results. M.N.R., L.A.K., P.L., and J.P.C. planned, performed, and analyzed the behavioral experiments. M.K.O.G. performed biochemistry experiments, including dot blots and size-exclusion chromatography. S.L.S. performed biochemistry experiments, including dot blots. P.L. and C.L.F. planned, performed, and analyzed the immunohistochemistry experiments. J.H.R. performed stereology-based quantification of amyloid load in Tg2576 mice. W.Q. prepared synthetic amyloid fibrils and characterized them by electron microscopy. A.C.A.C. treated and prepared tissue from TetO-APP_{SweInd} mice. J.L.J. supplied tissue from TetO-APP_{SweInd} mice and contributed to the interpretation of results. P.L., C.M.W., K.R.Z., and K.H.A. wrote the paper.

ACKNOWLEDGMENTS

The authors thank Dr. David Bennett, Rush University Medical Center, for providing human brain specimens; Dr. Sylvain Lesné and Mathew Sherman for providing aqueous extracts of human brains; and Dr. Robert Tycko for valuable advice. This work was supported by the National Institute for Neurological Diseases and Stroke (NS33249) and a gift from B. Grossman (K.H.A.), a grant from the Robert A. and Renee E. Belfer Family Foundation (J.L.J.), and the NIH intramural research program (W.Q.).

Received: March 31, 2015
Revised: May 4, 2015
Accepted: May 10, 2015
Published: June 4, 2015

REFERENCES

Alzforum (2015a). Bapineuzumab. http://www.alzforum.org/therapeutics/bapineuzumab.

Alzforum (2015b). Gantenerumab. http://www.alzforum.org/therapeutics/gantenerumab.

Benilova, I., Karran, E., and De Strooper, B. (2012). The toxic Aβ oligomer and Alzheimer's disease: an emperor in need of clothes. Nat. Neurosci. *15*, 349–357.

Billings, L.M., Green, K.N., McGaugh, J.L., and LaFerla, F.M. (2007). Learning decreases A beta*56 and tau pathology and ameliorates behavioral decline in 3xTg-AD mice. J. Neurosci. *27*, 751–761.

Bolmont, T., Haiss, F., Eicke, D., Radde, R., Mathis, C.A., Klunk, W.E., Kohsaka, S., Jucker, M., and Calhoun, M.E. (2008). Dynamics of the microglial/amyloid interaction indicate a role in plaque maintenance. J. Neurosci. *28*, 4283–4292.

Cheng, I.H., Scearce-Levie, K., Legleiter, J., Palop, J.J., Gerstein, H., Bien-Ly, N., Puoliväli, J., Lesné, S., Ashe, K.H., Muchowski, P.J., and Mucke, L. (2007). Accelerating amyloid-beta fibrillization reduces oligomer levels and functional deficits in Alzheimer disease mouse models. J. Biol. Chem. *282*, 23818–23828.

Cirrito, J.R., Yamada, K.A., Finn, M.B., Sloviter, R.S., Bales, K.R., May, P.C., Schoepp, D.D., Paul, S.M., Mennerick, S., and Holtzman, D.M. (2005). Synaptic activity regulates interstitial fluid amyloid-beta levels in vivo. Neuron *48*, 913–922.

Cohen, S.I., Linse, S., Luheshi, L.M., Hellstrand, E., White, D.A., Rajah, L., Otzen, D.E., Vendruscolo, M., Dobson, C.M., and Knowles, T.P. (2013). Proliferation of amyloid-β42 aggregates occurs through a secondary nucleation mechanism. Proc. Natl. Acad. Sci. USA *110*, 9758–9763.

Fowler, S.W., Chiang, A.C., Savjani, R.R., Larson, M.E., Sherman, M.A., Schuler, D.R., Cirrito, J.R., Lesné, S.E., and Jankowsky, J.L. (2014). Genetic modulation of soluble Aβ rescues cognitive and synaptic impairment in a mouse model of Alzheimer's disease. J. Neurosci. *34*, 7871–7885.

Glabe, C.G. (2008). Structural classification of toxic amyloid oligomers. J. Biol. Chem. *283*, 29639–29643.

Glabe, C.G. (2009). Amyloid oligomer structures and toxicity. Open Biol. J. *2*, 222–227.

Hsiao, K., Chapman, P., Nilsen, S., Eckman, C., Harigaya, Y., Younkin, S., Yang, F., and Cole, G. (1996). Correlative memory deficits, Abeta elevation, and amyloid plaques in transgenic mice. Science *274*, 99–102.

Jankowsky, J.L., Slunt, H.H., Gonzales, V., Savonenko, A.V., Wen, J.C., Jenkins, N.A., Copeland, N.G., Younkin, L.H., Lester, H.A., Younkin, S.G., and Borchelt, D.R. (2005). Persistent amyloidosis following suppression of Abeta production in a transgenic model of Alzheimer disease. PLoS Med. *2*, e355.

Kamenetz, F., Tomita, T., Hsieh, H., Seabrook, G., Borchelt, D., Iwatsubo, T., Sisodia, S., and Malinow, R. (2003). APP processing and synaptic function. Neuron *37*, 925–937.

Katzman, R., Terry, R., DeTeresa, R., Brown, T., Davies, P., Fuld, P., Renbing, X., and Peck, A. (1988). Clinical, pathological, and neurochemical changes in dementia: a subgroup with preserved mental status and numerous neocortical plaques. Ann. Neurol. *23*, 138–144.

Kawarabayashi, T., Younkin, L.H., Saido, T.C., Shoji, M., Ashe, K.H., and Younkin, S.G. (2001). Age-dependent changes in brain, CSF, and plasma amyloid (β) protein in the Tg2576 transgenic mouse model of Alzheimer's disease. J. Neurosci. *21*, 372–381.

Kayed, R., Head, E., Thompson, J.L., McIntire, T.M., Milton, S.C., Cotman, C.W., and Glabe, C.G. (2003). Common structure of soluble amyloid oligomers implies common mechanism of pathogenesis. Science *300*, 486–489.

Kayed, R., Head, E., Sarsoza, F., Saing, T., Cotman, C.W., Necula, M., Margol, L., Wu, J., Breydo, L., Thompson, J.L., et al. (2007). Fibril specific, conformation dependent antibodies recognize a generic epitope common to amyloid fibrils and fibrillar oligomers that is absent in prefibrillar oligomers. Mol. Neurodegener. *2*, 18.

Kotilinek, L.A., Westerman, M.A., Wang, Q., Panizzon, K., Lim, G.P., Simonyi, A., Lesne, S., Falinska, A., Younkin, L.H., Younkin, S.G., et al. (2008). Cyclooxygenase-2 inhibition improves amyloid-beta-mediated suppression of memory and synaptic plasticity. Brain *131*, 651–664.

Laganowsky, A., Liu, C., Sawaya, M.R., Whitelegge, J.P., Park, J., Zhao, M., Pensalfini, A., Soriaga, A.B., Landau, M., Teng, P.K., et al. (2012). Atomic view of a toxic amyloid small oligomer. Science *335*, 1228–1231.

Lasagna-Reeves, C.A., Glabe, C.G., and Kayed, R. (2011). Amyloid-β annular protofibrils evade fibrillar fate in Alzheimer disease brain. J. Biol. Chem. *286*, 22122–22130.

Lee, E.B., Leng, L.Z., Zhang, B., Kwong, L., Trojanowski, J.Q., Abel, T., and Lee, V.M. (2006). Targeting amyloid-beta peptide (Abeta) oligomers by passive immunization with a conformation-selective monoclonal antibody improves learning and memory in Abeta precursor protein (APP) transgenic mice. J. Biol. Chem. *281*, 4292–4299.

Lesné, S., Koh, M.T., Kotilinek, L., Kayed, R., Glabe, C.G., Yang, A., Gallagher, M., and Ashe, K.H. (2006). A specific amyloid-beta protein assembly in the brain impairs memory. Nature *440*, 352–357.

Lesné, S., Kotilinek, L., and Ashe, K.H. (2008). Plaque-bearing mice with reduced levels of oligomeric amyloid-beta assemblies have intact memory function. Neuroscience *151*, 745–749.

Lesné, S.E., Sherman, M.A., Grant, M., Kuskowski, M., Schneider, J.A., Bennett, D.A., and Ashe, K.H. (2013). Brain amyloid-β oligomers in ageing and Alzheimer's disease. Brain *136*, 1383–1398.

Liu, P., Kemper, L.J., Wang, J., Zahs, K.R., Ashe, K.H., and Pasinetti, G.M. (2011). Grape seed polyphenolic extract specifically decreases aβ*56 in the brains of Tg2576 mice. J. Alzheimers Dis. *26*, 657–666.

Liu, C., Zhao, M., Jiang, L., Cheng, P.N., Park, J., Sawaya, M.R., Pensalfini, A., Gou, D., Berk, A.J., Glabe, C.G., et al. (2012). Out-of-register β-sheets suggest a pathway to toxic amyloid aggregates. Proc. Natl. Acad. Sci. USA *109*, 20913–20918.

Liu, P., Paulson, J.B., Forster, C.L., Shapiro, S.L., Ashe, K.H., and Zahs, K.R. (2015). Characterization of a novel mouse model of Alzheimer's disease-amyloid pathology and unique β-amyloid oligomer profile. PLoS ONE *10*, e0126317.

Lu, J.X., Qiang, W., Yau, W.M., Schwieters, C.D., Meredith, S.C., and Tycko, R. (2013). Molecular structure of β-amyloid fibrils in Alzheimer's disease brain tissue. Cell *154*, 1257–1268.

Morris, R. (2007). Theories of hippocampal function. In The Hippocampus Book, P. Andersen, R. Morris, D. Amaral, T. Bliss, and J. O'Keefe, eds. (Oxford: Oxford University Press), pp. 581–694.

Noguchi, A., Matsumura, S., Dezawa, M., Tada, M., Yanazawa, M., Ito, A., Akioka, M., Kikuchi, S., Sato, M., Ideno, S., et al. (2009). Isolation and characterization of patient-derived, toxic, high mass amyloid beta-protein (Abeta) assembly from Alzheimer disease brains. J. Biol. Chem. *284*, 32895–32905.

Ostrowitzki, S., Deptula, D., Thurfjell, L., Barkhof, F., Bohrmann, B., Brooks, D.J., Klunk, W.E., Ashford, E., Yoo, K., Xu, Z.X., et al. (2012). Mechanism of amyloid removal in patients with Alzheimer disease treated with gantenerumab. Arch. Neurol. *69*, 198–207.

Paule, M.G., Bushnell, P.J., Maurissen, J.P., Wenger, G.R., Buccafusco, J.J., Chelonis, J.J., and Elliott, R. (1998). Symposium overview: the use of delayed matching-to-sample procedures in studies of short-term memory in animals and humans. Neurotoxicol. Teratol. *20*, 493–502.

Paulson, J.B., Ramsden, M., Forster, C., Sherman, M.A., McGowan, E., and Ashe, K.H. (2008). Amyloid plaque and neurofibrillary tangle pathology in a regulatable mouse model of Alzheimer's disease. Am. J. Pathol. *173*, 762–772.

Perez-Nievas, B.G., Stein, T.D., Tai, H.C., Dols-Icardo, O., Scotton, T.C., Barroeta-Espar, I., Fernandez-Carballo, L., de Munain, E.L., Perez, J., Marquie, M., et al. (2013). Dissecting phenotypic traits linked to human resilience to Alzheimer's pathology. Brain *136*, 2510–2526.

Qiang, W., Yau, W.M., Luo, Y., Mattson, M.P., and Tycko, R. (2012). Antiparallel β-sheet architecture in Iowa-mutant β-amyloid fibrils. Proc. Natl. Acad. Sci. USA *109*, 4443–4448.

Reed, M.N., Hofmeister, J.J., Jungbauer, L., Welzel, A.T., Yu, C., Sherman, M.A., Lesné, S., LaDu, M.J., Walsh, D.M., Ashe, K.H., and Cleary, J.P. (2011). Cognitive effects of cell-derived and synthetically derived Aβ oligomers. Neurobiol. Aging *32*, 1784–1794.

Rinne, J.O., Brooks, D.J., Rossor, M.N., Fox, N.C., Bullock, R., Klunk, W.E., Mathis, C.A., Blennow, K., Barakos, J., Okello, A.A., et al. (2010). 11C-PiB PET assessment of change in fibrillar amyloid-beta load in patients with Alzheimer's disease treated with bapineuzumab: a phase 2, double-blind, placebo-controlled, ascending-dose study. Lancet Neurol. *9*, 363–372.

Rozkalne, A., Spires-Jones, T.L., Stern, E.A., and Hyman, B.T. (2009). A single dose of passive immunotherapy has extended benefits on synapses and neurites in an Alzheimer's disease mouse model. Brain Res. *1280*, 178–185.

Serrano-Pozo, A., Frosch, M.P., Masliah, E., and Hyman, B.T. (2011). Neuropathological alterations in Alzheimer disease. Cold Spring Harb. Perspect. Med. *1*, a006189.

Sgourakis, N.G., Yau, W.M., and Qiang, W. (2015). Modeling an in-register, parallel "iowa" aβ fibril structure using solid-state NMR data from labeled samples with rosetta. Structure *23*, 216–227.

Shankar, G.M., Li, S., Mehta, T.H., Garcia-Munoz, A., Shepardson, N.E., Smith, I., Brett, F.M., Farrell, M.A., Rowan, M.J., Lemere, C.A., et al. (2008). Amyloid-beta protein dimers isolated directly from Alzheimer's brains impair synaptic plasticity and memory. Nat. Med. *14*, 837–842.

Shankar, G.M., Leissring, M.A., Adame, A., Sun, X., Spooner, E., Masliah, E., Selkoe, D.J., Lemere, C.A., and Walsh, D.M. (2009). Biochemical and immunohistochemical analysis of an Alzheimer's disease mouse model reveals the presence of multiple cerebral Abeta assembly forms throughout life. Neurobiol. Dis. *36*, 293–302.

Strobel, G. (2015). Biogen antibody buoyed by Phase 1 data and hungry investors. http://www.alzforum.org/news/conference-coverage/biogen-antibody-buoyed-phase-1-data-and-hungry-investors.

Terry, R.D., Masliah, E., Salmon, D.P., Butters, N., DeTeresa, R., Hill, R., Hansen, L.A., and Katzman, R. (1991). Physical basis of cognitive alterations in Alzheimer's disease: synapse loss is the major correlate of cognitive impairment. Ann. Neurol. *30*, 572–580.

Tycko, R. (2011). Solid-state NMR studies of amyloid fibril structure. Annu. Rev. Phys. Chem. *62*, 279–299.

van Haaren, F., van Zijderveld, G., van Hest, A., de Bruin, J.P., van Eden, C.G., and van de Poll, N.E. (1988). Acquisition of conditional associations and operant delayed spatial response alternation: effects of lesions in the medial prefrontal cortex. Behav. Neurosci. *102*, 481–488.

Westerman, M.A., Cooper-Blacketer, D., Mariash, A., Kotilinek, L., Kawarabayashi, T., Younkin, L.H., Carlson, G.A., Younkin, S.G., and Ashe, K.H. (2002). The relationship between Abeta and memory in the Tg2576 mouse model of Alzheimer's disease. J. Neurosci. *22*, 1858–1867.

Wright, A.L., Zinn, R., Hohensinn, B., Konen, L.M., Beynon, S.B., Tan, R.P., Clark, I.A., Abdipranoto, A., and Vissel, B. (2013). Neuroinflammation and neuronal loss precede Aβ plaque deposition in the hAPP-J20 mouse model of Alzheimer's disease. PLoS ONE *8*, e59586.

Wu, J.W., Breydo, L., Isas, J.M., Lee, J., Kuznetsov, Y.G., Langen, R., and Glabe, C. (2010). Fibrillar oligomers nucleate the oligomerization of monomeric amyloid beta but do not seed fibril formation. J. Biol. Chem. *285*, 6071–6079.